PERGAMON

Applied Mathematics Letters 12 (1999) 89–96

Applied Mathematics Letters

A Modified Structured Central Scheme for 2D Hyperbolic Conservation Laws

T. KATSAOUNIS AND D. LEVY
Département de Mathématiques et d'Informatique
Ecole Normale Supérieure, 45 rue d'Ulm, 75230 Paris Cedex 05, France
<katsaoun><dlevy>@dmi.ens.fr

(Received and accepted June 1998)

Communicated by B. Wendroff

Abstract—We present a new central scheme for approximating solutions of two-dimensional systems of hyperbolic conservation laws. This method is based on a modification of the staggered grid proposed in [1] which prevents the crossings of discontinuities in the normal direction, while retaining the simplicity of the central framework. Our method satisfies a local maximum principle which is based on a more compact stencil. Unlike the previous method, it enables a natural extension to adaptive methods on structured grids.

Keywords—Hyperbolic conservation laws, Central difference schemes, Nonoscillatory schemes, Adaptive methods.

1. INTRODUCTION

In [1], Jiang and Tadmor presented a second-order two-dimensional central scheme for approximating solutions of systems of hyperbolic conservation laws which extends the one-dimensional Nessyahu-Tadmor (NT) scheme, see [2]. A similar approach was taken by Arminjon, *et al.* in [3,4].

Following the central framework whose prototype is the Lax and Friedrichs scheme [5], a Godunov-type scheme was constructed. First, a piecewise-linear MUSCL-type [6] interpolant was reconstructed from the given cell-averages. Spurious oscillations in the reconstruction were avoided by implementing a nonlinear limiting mechanism [7]. This interpolant was then evolved exactly in time and finally projected on its staggered cell-averages. Due to the staggering, there was no need to solve two-dimensional Riemann problems. Unfortunately, the staggering was not sufficient to eliminate the discontinuities from the problem, and one was actually left with one-dimensional Riemann problems in the normal direction. In the method proposed in [1], instead of explicitly solving these 1D Riemann problems, the values around the discontinuities were averaged. The dissipative treatment of those discontinuities in the normal direction resulted in several numerical consequences such as smearing of the discontinuities as evident in the numerical results presented in [1].

In this work, we present a new central scheme which was designed to *avoid the crossings of discontinuities in the normal direction.* Our goal is obtained by exchanging the original staggered

0893-9659/99/$ - see front matter. Typeset by AMS-TEX
PII: S0893-9659(99)00084-1

mesh with an alternative rotated and stretched mesh. All that follows, is a direct implementation of the previously designed methods with our new meshes. This new structured mesh can be viewed as a degenerate version of the unstructured mesh used in [8].

Along with the main advantage of our new method, several byproducts are in hand. First, the method in [1] when viewed in every two time steps consisted of a 9-point stencil. Our method, however, is based on a more *compact* 5-point stencil. Moreover, unlike the method in [1], our new method can be easily extended to *adaptive* central schemes which are based on *structured* staggered grids. Such an extension seems to be highly nontrivial in the previous framework.

This paper is organized as follows. We start in Section 2 by presenting our new central method. The simplicity compared with an adaptive unstructured framework is emphasized by the explicit formulation of the method outlined below. We then proceed in Section 3 to formulate and prove a maximum principle on the scheme. We end in Section 4 with several numerical examples.

2. THE 2D METHOD

We consider the two-dimensional system of conservation laws

$$v_t + f(v)_x + g(v)_y = 0, \tag{2.1}$$

augmented with the initial data, $v_0(x,y) = v(x,y,t=0)$. To approximate solutions of (2.1), we first introduce a uniform rectangular mesh in the (x,y) plane, with spacings taken as $\Delta x, \Delta y$. On top of this mesh, we then build a staggered mesh, whose cells are of the shape of diamonds, consult Figure 1a.

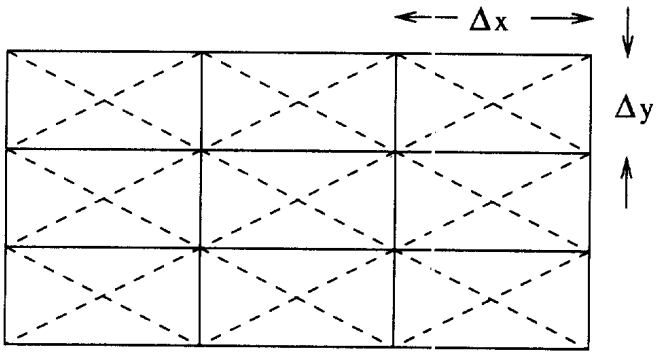

(a) The staggered mesh. Solid lines—rectangular grid. Dotted lines—diamond-shaped grid.

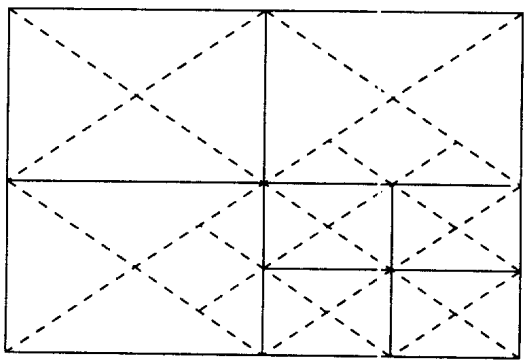

(b) A structured adaptive grid.

Figure 1.

By Ω_i and $\tilde{\Omega}_i$, we denote the rectangular cells and the diamond cells, respectively. The resulting meshes are, therefore, abbreviated as $\Omega = \bigcup_i \Omega_i$ and $\tilde{\Omega} = \bigcup_i \tilde{\Omega}_i$. For simplicity of notations, we use a fixed time-step Δt, and denote the discrete time by $t^n = n\Delta t$. By $\bar{u}^n_{\Omega_i}$, we denote

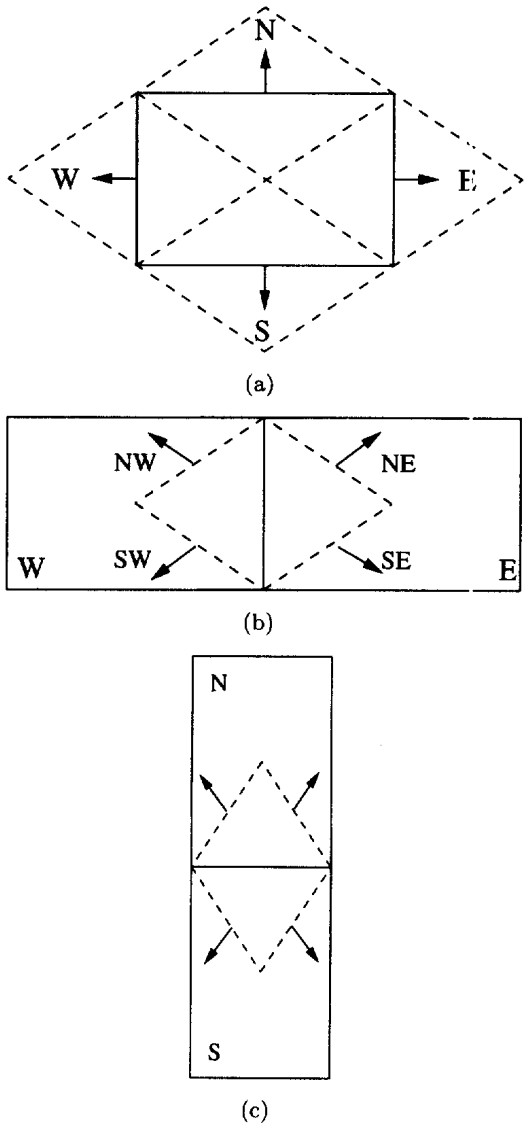

Figure 2. Reconstruction: (a) squares from diamonds, (b) and (c) diamonds from squares.

an approximation to the cell-average $\bar{v}^n_{\Omega_i}$ in cell Ω_i and at time t^n. In the first phase of the staggering, we assume that $\bar{u}^n_{\tilde{\Omega}_i}$ are given and we wish to compute $\bar{u}^{n+1}_{\Omega_i}$. In the second phase, the roles of $\tilde{\Omega}$ and Ω are exchanged.

The reconstruction of our Godunov-type second-order method starts by reconstructing a piecewise-linear interpolant from the given cell-averages

$$u(x,y,t^n) = \sum_{\tilde{\Omega}_i} P_i(x,y,t^n)\chi_{\tilde{\Omega}_i}. \tag{2.2}$$

Here, $\chi_{\tilde{\Omega}_i}$ denoted the characteristic function of the cell $\tilde{\Omega}_i$ while P_i is a linear polynomial

$$P_i(x,y,t^n) = \bar{u}^n_{\tilde{\Omega}_i} + u'_{\tilde{\Omega}_i}\left(\frac{x-x_{c_i}}{\Delta x}\right) + u'_{\tilde{\Omega}_i}\left(\frac{y-y_{c_i}}{\Delta y}\right),$$

where the center of $\tilde{\Omega}_i$ is denoted by (x_{c_i}, y_{c_i}), and $u'_{\tilde{\Omega}_i}$, $u'_{\tilde{\Omega}_i}$, are the discrete slopes in the x- and y-directions, respectively, $u'_{\tilde{\Omega}_i} \sim \Delta x \cdot u_x(x_{c_i}, y_{c_i}, t^n) + O(\Delta x)^2$, $u'_{\tilde{\Omega}_i} \sim \Delta y \cdot u_y(x_{c_i}, y_{c_i}, t^n) + O(\Delta y)^2$. The reconstruction of the slopes utilizes nonlinear limiters described in the remarks below.

An exact evolution of (2.2) followed by a projection on its staggered cell-averages results with (consult Figure 2a)

$$\bar{u}^{n+1}_{\Omega_i} = \bar{u}^{n}_{\Omega_i} - \frac{1}{|\Omega_i|}\int_{t^n}^{t^{n+1}} \left[\iint_{\Omega_i} f_x + \iint_{\Omega_i} g_y\right] dx\,dy\,d\tau := \mathcal{I}_1 + \mathcal{I}_2. \tag{2.3}$$

The first term of the RHS of (2.3), $\mathcal{I}_1$, equals

$$\mathcal{I}_1 = \bar{u}^{n}_{\Omega_i} = \frac{\bar{u}^{n}_{\mathrm{N}} + \bar{u}^{n}_{\mathrm{E}} + \bar{u}^{n}_{\mathrm{S}} + \bar{u}^{n}_{\mathrm{W}}}{4} + \frac{1}{24}\left[\Delta x\left(u'_{\mathrm{W}} - u'_{\mathrm{E}}\right) + \Delta y\left(u'_{\mathrm{S}} - u'_{\mathrm{N}}\right)\right].$$

The integrals over the fluxes in the second term of the RHS of (2.3), $\mathcal{I}_2$, are approximated by a second-order midpoint quadrature rule, an approximation which is valid as long as it is done in a smooth region. The smoothness requirement results with a CFL condition on the stability of the method which due to geometric consideration equals 1/4 (compared with 1/2 in [1]). This quadrature can be then explicitly written as

$$\mathcal{I}_2 = -\lambda\left[f\left(u^{n+1/2}_{\mathrm{E}}\right) - f\left(u^{n+1/2}_{\mathrm{W}}\right)\right] - \mu\left[g\left(u^{n+1/2}_{\mathrm{N}}\right) - g\left(u^{n+1/2}_{\mathrm{S}}\right)\right], \tag{2.4}$$

where $\lambda = \Delta t/\Delta x$ and $\mu = \Delta t/\Delta y$ are the usual fixed mesh ratios. The values at time $t^{n+1/2}$ required in (2.4) are predicted using a first-order Taylor expansion (which is sufficient for overall second-order accuracy due to the predictor-corrector structure of the method). Hence, for example, $u^{n+1/2}_{\mathrm{E}} = \bar{u}^{n}_{\mathrm{E}} - (\lambda/2)f(u_{\mathrm{E}})' - (\mu/2)g(u_{\mathrm{E}})'$, and analogously for the other intermediate values.

In the second phase of the staggering, we assume that the values, $\bar{u}^{n}_{\tilde{\Omega}}$ are known and we wish to compute $\bar{u}^{n+1}_{\tilde{\Omega}}$. In order to simplify the notations, we again advance in time from time t^n to t^{n+1}. The computation is analogous to the first phase, only this time due to the lack of symmetry between the two phases of the staggering, the resulting formulas are different. Here, there are two possibilities which are schematically drawn in Figures 2b and 2c. For both cases, an exact evolution in time of our reconstruction, $u(x,y,t^n) := \sum_{\Omega_i} P_i(x,y,t^n)\chi_{\Omega_i}$, yields (compare with (2.3)),

$$\bar{u}^{n+1}_{\tilde{\Omega}_i} = \bar{u}^{n}_{\tilde{\Omega}_i} - \frac{1}{|\tilde{\Omega}_i|}\int_{t^n}^{t^{n+1}} \left[\iint_{\tilde{\Omega}_i} f_x + \iint_{\tilde{\Omega}_i} g_y\right] dx\,dy\,d\tau := \mathcal{I}_1 + \mathcal{I}_2. \tag{2.5}$$

We start with the case described in Figure 2b. Here, $\mathcal{I}_1 = \bar{u}^{n}_{\tilde{\Omega}_i} = (\bar{u}^{n}_{\mathrm{W}} + \bar{u}^{n}_{\mathrm{E}}/2) + (\Delta x/6)(u'_{\mathrm{W}} - u'_{\mathrm{E}})$, and

$$\mathcal{I}_2 = -\sqrt{\lambda^2+\mu^2}\cdot\sum_{\partial_j\tilde{\Omega}_i}\left[f\left(u^{n+1/2}_{\partial^c_j\tilde{\Omega}_i}\right)\cdot\vec{n}_x + g\left(u^{n+1/2}_{\partial^c_j\tilde{\Omega}_i}\right)\cdot\vec{n}_y\right]. \tag{2.6}$$

The midvalues, $u^{n+1/2}_{\partial^c_j\tilde{\Omega}_i}$, required in (2.6) are once again predicted by Taylor expansion

$$u^{n+1/2}_{\partial^c_j\tilde{\Omega}_i} = u^{n}_{\partial^c_j\tilde{\Omega}_i} - \frac{\Delta t}{2}\left[f_u\left(u^{n}_{\partial^c_j\tilde{\Omega}_i}\right)\cdot u'_{\partial^c_j\tilde{\Omega}_i} + g_u\left(u^{n}_{\partial^c_j\tilde{\Omega}_i}\right)\cdot u'_{\partial^c_j\tilde{\Omega}_i}\right],$$

where $\partial^c_j\tilde{\Omega}_i$ represents the center of the edges of the diamond cells, $j = \{\mathrm{NE}, \mathrm{SE}, \mathrm{NW}, \mathrm{SW}\}$ (see Figure 2b). Here, $\mathcal{D}u_{\mathrm{NE}} = \mathcal{D}u_{\mathrm{SE}} = \mathcal{D}u_{\mathrm{E}}$ and $\mathcal{D}u_{\mathrm{NW}} = \mathcal{D}u_{\mathrm{SW}} = \mathcal{D}u_{\mathrm{W}}$, with $\mathcal{D}$ denoting the discrete derivative either in the x- or in the y-direction. The point-values, $u^{n}_{\partial^c_j\tilde{\Omega}_i}$, are also computed by a Taylor expansion, e.g., $u^{n}_{\mathrm{NE}} = u^{n}_{\mathrm{E}} - (\Delta x/4)u'_{\mathrm{E}} + (\Delta y/4)u'_{\mathrm{E}}$.

Analogous computations hold for the last case described in Figure 2c. For the sake of brevity, we list only the first term on the RHS of (2.5), $\mathcal{I}_1$, which in this case equals $\mathcal{I}_1 = \bar{u}^{n}_{\tilde{\Omega}_i} = (\bar{u}^{n}_{\mathrm{N}} + \bar{u}^{n}_{\mathrm{S}}/2) + (\Delta y/6)(u'_{\mathrm{S}} - u'_{\mathrm{N}})$.

REMARKS.

1. Reconstruction of the Derivatives. A reconstruction of the derivatives without creating spurious oscillations requires nonlinear built-in limiters. One can use, for example, for the x-derivative in a rectangular cell (j,k), a limiting on the right/centered/left derivatives

$$u'_{j,k} = \mathrm{MM}\left\{\theta\left(\bar{u}^n_{j+1,k} - \bar{u}^n_{j,k}\right), \frac{1}{2}\left(\bar{u}^n_{j+1,k} - \bar{u}^n_{j-1,k}\right), \theta\left(\bar{u}^n_{j,k} - \bar{u}^n_{j-1,k}\right)\right\}, \tag{2.7}$$

with $1 \le \theta \le 2$, and

$$\mathrm{MM}\left\{u1, u2, \ldots\right\} = \begin{cases} \min_i\{u_i\}, & \text{if } v_i > 0, \quad \forall i, \\ \max_i\{u_i\}, & \text{if } v_i < 0, \quad \forall i, \\ 0, & \text{otherwise.} \end{cases}$$

The choice of $\theta = 1$ agrees with the classical Min-Mod limiter (see [1,7] for more details). Analogous expression holds for the y-derivative. The same routine is repeated for the derivatives in the diamond cells. Only this time, since the cells are not aligned with the axes, one has to limit the derivatives after *projecting* them on the x and y directions. For systems, the derivatives are computed component-wise, i.e., $f'_{j,k} = f_u(u_{j,k})u'_{j,k}$, where $u'_{j,k}$ are given by (2.7), consult [1,2].

2. Adaptive Mesh. A possible extension of the method to adaptive method on unstructured meshes is demonstrated in Figure 1b. An equivalent extension with the previous method in [1] seems to be impossible, at least without dealing with complicated cases at the boundaries (corners, etc.) and with uneven divisions of the cells. Our method formulated on the new mesh requires no special corner treatment. We consider this to be the great advantage of our method over the other available structured 2D methods. Moreover, since there is no upwinding involved, none of the reflected-waves problems which are typical to upwinding methods on adaptive structured meshes should appear.
3. Efficient Implementation. We note that the simplicity of the scheme can be directly projected onto its implementation. It is unnecessary to use the standard methods of the unstructured framework in order to implement our method. The simplest data structure to store the values in the diamonds would be to divide them into triangles and to store the values in the triangles in a two-dimensional array, such that every point in the array corresponds to the rectangle which these triangles belong to. In fact, the values of only two triangles out of four in each rectangle should be stored, as the values of the other two can be retrieved from the neighboring cells.

3. A MAXIMUM PRINCIPLE FOR SCALAR APPROXIMATIONS

An equivalent maximum principle to Theorem 1 in [1] implies to our new scheme. Since our scheme is nonsymmetric between the two phases of the staggering, it is natural to formulate the theorem in a nonstaggered version by considering two joint time-steps. This results with a *local* bound on the cell-averages based on values taken from a 5-point stencil. An equivalent two time-steps formulation of Theorem 1 in [1] would be based on a 9-point stencil.

THEOREM 3.1. *Consider the two-dimensional scalar scheme (2.3),(2.5). Assume that the discrete slopes satisfy the limiter property (2.7). Then for any $1 \le \theta < 2$, there exists a sufficiently small CFL number C_θ, such that if the following CFL condition is fulfilled,*

$$\max\left(\lambda \cdot \max_u |f_u(u)|, \mu \cdot \max_u |g_u(u)|\right) \le C_\theta,$$

then the following local maximum principle holds:

$$\min\left\{\bar{u}^n_{j-1,k}, \bar{u}^n_{j,k}, \bar{u}^n_{j+1,k}, \bar{u}^n_{j,k-1}, \bar{u}^n_{j,k+1}\right\} \le \bar{u}^{n+2}_{j,k} \le \max\left\{\bar{u}^n_{j-1,k}, \bar{u}^n_{j,k}, \bar{u}^n_{j+1,k}, \bar{u}^n_{j,k-1}, \bar{u}^n_{j,k+1}\right\}.$$

The proof of Theorem 3.1 is analogous to the proof of [1, Theorem 1] and we omit it for brevity. The key observation for the proof is that every new staggered cell average can be written as a convex combination of sums and differences of the cell-averages in the supporting cells.

4. NUMERICAL EXAMPLES

In Table 1, we present the L_1 and L_∞ errors and convergence rate estimates for the linear oblique advection $v_t + v_x + v_y = 0$ subject to $v_0 = \sin(\pi(x+y))$. Equal spacings were used, $\Delta x = \Delta y = 1/N$. The CFL was taken as 0.2 and the time $T = 0.5$. We used the MM limiter with $\theta = 1$. These results are indeed comparable with those presented in [1, Table 4.1].

We end by presenting an example demonstrating the nonoscillatory behavior of our method. In Figure 3, we show the results obtained for the periodic two-dimensional Burgers' equation, $v_t + vv_x + vv_y = 0$ in $[-1,1] \times [-1,1]$, for time $T = 0.5$, subject to the initial conditions,

$$v_0(x,y) = \begin{cases} -1.0, & x < 0, y < 0, \\ -0.2, & x > 0, y < 0, \end{cases} \qquad v_0(x,y) = \begin{cases} 0.8, & x < 0, y > 0, \\ 0.5, & x > 0, y > 0. \end{cases}$$

The label JT refers to the method of [1]. The contour plots in Figure 3 are zoomed into $[0,1] \times [-1,0]$. Clearly, our method handles better 'diagonal' waves compared with the method of [1], while less smearing the discontinuities (compare the results of both methods for the same CFL).

Table 1. Linear oblique advection. L_1 and L_∞ errors and convergence rates.

N	L_1 Error	L_1 Order	L_∞ Error	L_∞ Order
20	0.334716	–	0.120738	–
40	0.020296	4.04	0.023076	2.39
80	0.005177	1.97	0.009852	1.23
160	0.001661	1.64	0.004155	1.25
320	0.000698	1.25	0.001740	1.26

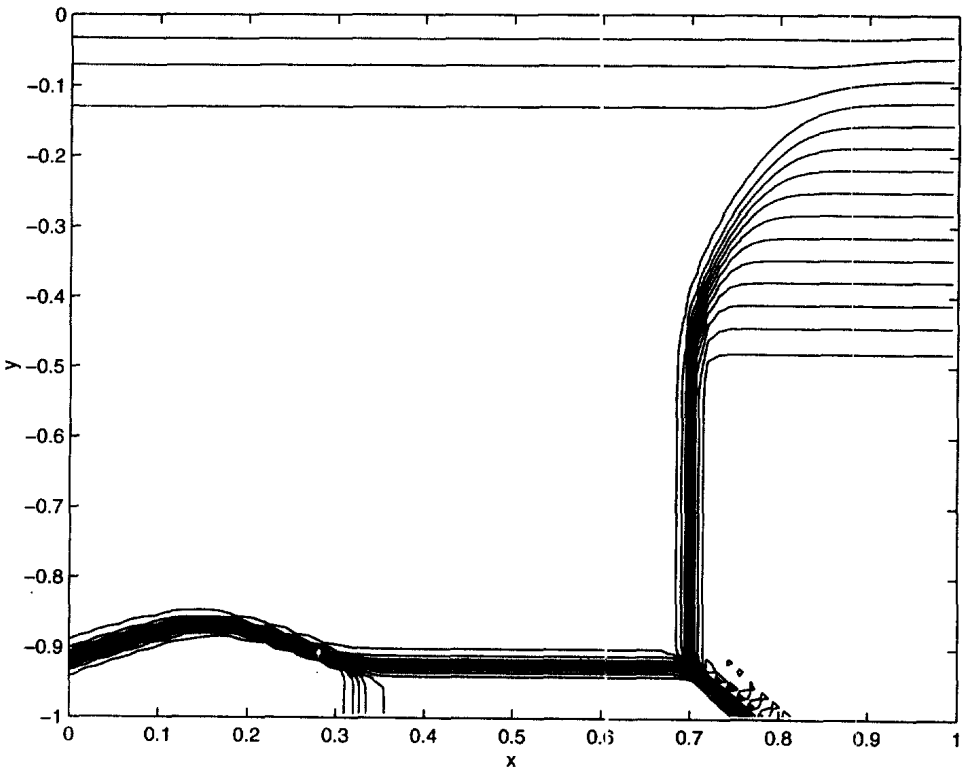

(a) JT, CFL=0.4.

Figure 3. Periodic 2D-burgers. $N = 160$.

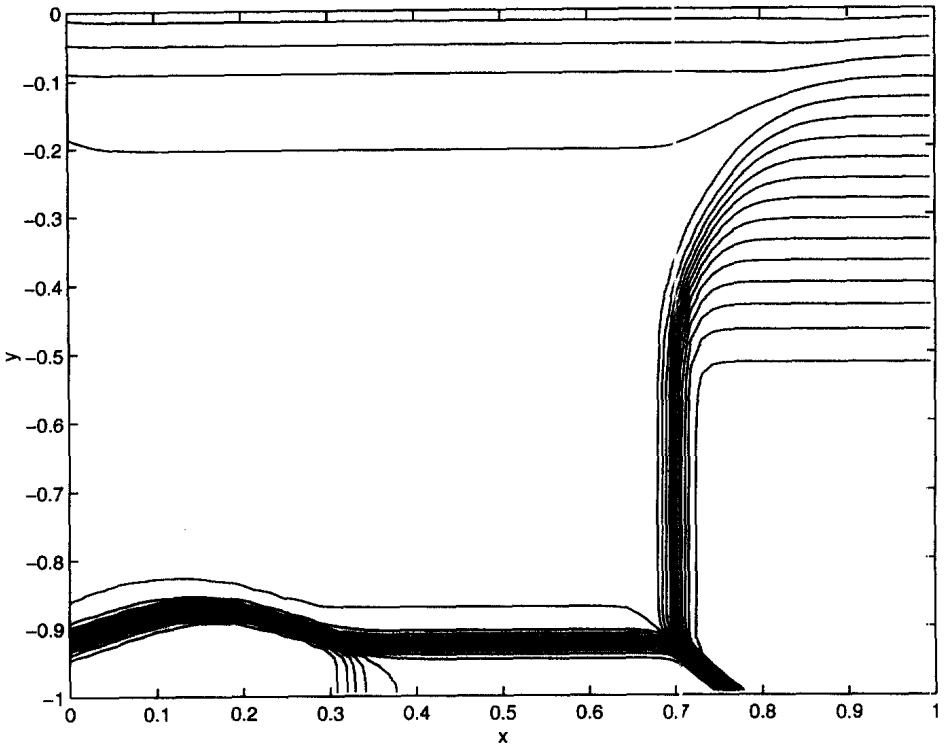

(b) JT, CFL=0.2.

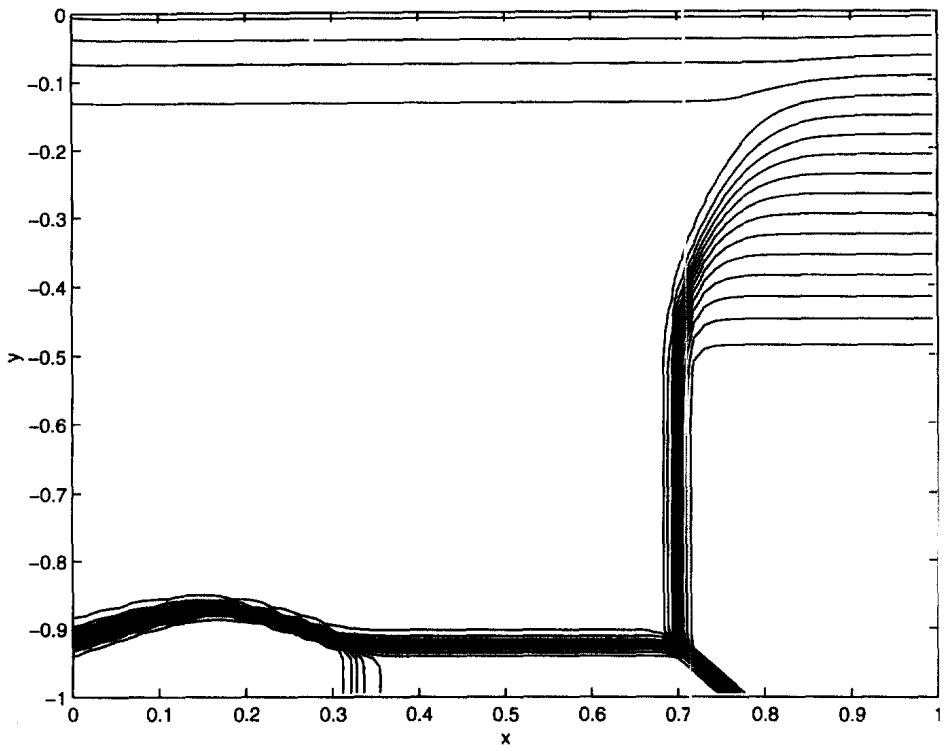

(c) The new method, CFL=0.2.

Figure 3 (cont.)

REFERENCES

1. G.-S. Jiang and E. Tadmor, Nonoscillatory central schemes for multidimensional hyperbolic conservation laws, *SIAM J. Sci. Comp.* (to appear).
2. H. Nessyahu and E. Tadmor, Non-oscillatory central differencing for hyperbolic conservation laws, *JCP* **87** (2), 408–463, (1990).

3. P. Arminjon, D. Stanescu and M.-C. Viallon, A two-dimensional finite volume extension of the Lax-Friedrichs and Nessyahu-Tadmor schemes for compressible flow, In *Proc. 6th Int. Symp. on CFD*, (Edited by M. Hafez and K. Oshima), Volume IV, pp. 7–14, Lake Tahoe, (1995).
4. P. Arminjon and M.-C. Viallon, Généralisation du Schéma de Nessyahu-Tadmor pour Une Équation Hyperbolique à Deux Dimensions D'espace, *C.R. Acad. Sci. Paris* **320** (Série I), 85–88, (1995).
5. K.O. Friedrichs and P.D. Lax, Systems of conservation equations with a convex extension, *Proc. Nat. Acad. Sci.* **68**, 1686–1688, (1971).
6. B. van Leer, Towards the ultimate conservative difference scheme, V. A second-order sequel to Godunov's method, *JCP* **32**, 101–136, (1979).
7. P.K. Sweby, High resolution schemes using flux limiters for hyperbolic conservation laws, *SINUM* **21** (5), 995–1011, (1984).
8. P. Arminjon, M.-C. Viallon and A. Madrane, A finite volume extension of the Lax-Friedrichs and Nessyahu-Tadmor schemes for conservation laws on unstructured grids, *IJCFD* **9**, 1–22, (1997).